International Journal of Pharmaceutics 658 (2024) 124215

Contents lists available at ScienceDirect

International Journal of Pharmaceutics

journal homepage: www.elsevier.com/locate/ijpharm

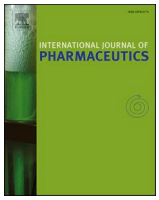

Amorphous solid dispersion of a binary formulation with felodipine and HPMC for 3D printed floating tablets

Gloria Mora-Castaño [a], Mónica Millán-Jiménez [a,*], Andreas Niederquell [b], Monica Schönenberger [c], Fatemeh Shojaie [a], Martin Kuentz [b], Isidoro Caraballo [a]

[a] Department of Pharmacy and Pharmaceutical Technology, Faculty of Pharmacy, Universidad de Sevilla, 41012 Seville, Spain
[b] School of Life Sciences, University of Applied Sciences and Arts Northwestern Switzerland, CH 4132 Muttenz, Switzerland
[c] University of Basel, Swiss Nanoscience Institute, Nano Imaging Lab, Klingelbergstrasse 82, 4056 Basel, Switzerland

ARTICLE INFO

Keywords:
Amorphous solid dispersion
3D printing
Fused deposition modeling
Gastroretentive floating tablets
Drug-loaded filaments
Zero-order release

ABSTRACT

This study focuses on the combination of three-dimensional printing (3DP) and amorphous solid dispersion (ASD) technologies for the manufacturing of gastroretentive floating tablets. Employing hot melt extrusion (HME) and fused deposition modeling (FDM), the study investigates the development of drug-loaded filaments and 3D printed (3DP) tablets containing felodipine as model drug and hydroxypropyl methylcellulose (HPMC) as the polymeric carrier. Prior to fabrication, solubility parameter estimation and molecular dynamics simulations were applied to predict drug-polymer interactions, which are crucial for ASD formation. Physical bulk and surface characterization complemented the quality control of both drug-loaded filaments and 3DP tablets. The analysis confirmed a successful amorphous dispersion of felodipine within the polymeric matrix. Furthermore, the low infill percentage and enclosed design of the 3DP tablet allowed for obtaining low-density systems. This structure resulted in buoyancy during the entire drug release process until a complete dissolution of the 3DP tablets (more than 8 h) was attained. The particular design made it possible for a single polymer to achieve a zero-order controlled release of the drug, which is considered the ideal kinetics for a gastroretentive system. Accordingly, this study can be seen as an advancement in ASD formulation for 3DP technology within pharmaceutics.

1. Introduction

Three-dimensional printing (3DP) is an innovative additive manufacturing technique capable of converting 3D computer models into real objects through the sequential deposition of material layer by layer. The ability to manufacture complex structures has opened new possibilities in the design of pharmaceutical dosage forms with different shapes, sizes, dosages, as well as drug release characteristics and multiple drug combinations (Ayyoubi et al., 2021; dos Santos et al., 2023; Parulski et al., 2022; Sadia et al., 2018; Shojaie et al., 2023; Verstraete et al., 2018; Zhang et al., 2017). Three-dimensional printing offers a solution to a major drawback of conventional gastroretentive drug delivery systems (GDDS), which is the limitation of the tablet design. With 3D printing, it is possible to design personalized dosage forms with complex geometries and specific characteristics to improve gastric retention and controlled release of the drug in the stomach. It allows the density and composition of the formulation to be precisely adjusted, which can be beneficial in achieving controlled flotation in the gastric environment (Dumpa et al., 2020; Huanbutta and Sangnim, 2019; Khizer et al., 2023; Melocchi et al., 2021; Mora-Castaño et al., 2023). 3DP is introducing a new approach to personalized treatment, as it enables pharmaceutical forms to be manufactured adapted to the individual needs of patients.

Currently, one of the most evaluated 3DP techniques in the pharmaceutical area is fused deposition modeling (FDM), due to the low cost of the printer, the good quality of the final product, high reproducibility, and the potential for innovative drug management strategies. FDM is based on the extrusion of a filament from a heated extrusion head through a nozzle. In this process, materials are melted and deposited layer by layer on a platform that moves in the x and y axes. As the plate descends, the object is built from the bottom up. The ability to precisely control processing parameters allows FDM to have enormous potential and utility for the preparation of personalized medicine (Cailleaux et al., 2021; Dumpa et al., 2021; Melocchi et al., 2021; Pereira and Figueiredo,

* Corresponding author.
E-mail address: momillan@us.es (M. Millán-Jiménez).

https://doi.org/10.1016/j.ijpharm.2024.124215
Received 1 March 2024; Received in revised form 19 April 2024; Accepted 7 May 2024
Available online 11 May 2024

2020).

However, one of the main drawbacks of FDM is that it requires prior preparation of drug-loaded filaments, usually by hot melt extrusion (HME) (Bandari et al., 2021; Mora-Castaño et al., 2022; Zhao et al., 2022). The high dependence on the physical and mechanical properties of the filaments for the viability of printing and the difficulty of filament preparation are the main drawbacks of this technology (Bandari et al., 2021; Mora-Castaño et al., 2022). HME is a process in which a blend of materials, mainly polymers, drugs, and eventual additives, is melted or softened under elevated temperature and pressure to pass under force along a barrel containing rotating screws. The final product emerges from the barrel through a die that shapes the extruded product (Tan et al., 2018). HME offers many advantages, such as the absence of organic solvents and a low number of processing steps. The possibility of continuous processing and scalability allows its use for pharmaceutical development (Alzahrani et al., 2022; Bandari et al., 2021; Jennotte et al., 2022; Tambe et al., 2021).

HME and 3D extrusion-based printing technologies are also innovative tools for formulating amorphous solid dispersions (ASDs), which consist of amorphous drugs dispersed and stabilized on a polymeric support (Bhujbal et al., 2021). Obtaining ASD formulations is a strategy to improve the apparent solubility of drugs and potentially increase their absorption and bioavailability (Alzahrani et al., 2022; Yani et al., 2017).

Among the drawbacks that ASDs present, we can highlight the risk of degradation due to hydrolysis or oxidation, as the amorphous drug is more hygroscopic than its crystalline form, and the possibility of drug recrystallization. These drawbacks can be overcome by stabilizing the amorphous drug with a carrier, usually a polymer (Jennotte et al., 2022). The polymer must have the ability to raise the energy threshold necessary for the nucleation and crystallization of the drug and decrease the mobility of the molecules. These mechanisms inhibit drug crystallization during dissolution tests, maintaining the supersaturation state (Jennotte et al., 2022; Vo et al., 2017; Xiang and Anderson, 2017).

Factors such as drug-polymer miscibility, solubility of the drug in the polymer, residual crystallinity, molecular mobility, drug-polymer interaction, and the manufacturing process also influence the stability of ASDs, as well as the temperature and humidity of storage. (Alzahrani et al., 2022).

A rational approach is preferred to select suitable drugs and excipients for manufacturing ASD, thereby reducing time to market and minimizing costs associated with development (DeBoyace and Wildfong, 2018; Han et al., 2019; Tambe et al., 2022; Zhang et al., 2023). Understanding and predicting the miscibility between the carrier and the drug is a crucial aspect of ASDs to ensure the physical stability of the drug (Xiang and Anderson, 2017; Zhang et al., 2023).

Different analytical technologies used to characterize the amorphous solid state (Deon et al., 2022) and verify the results obtained in theoretical predictions made in previous stages are valuable tools. Confirming the compatibility and miscibility of the components of the amorphous dispersion is essential to ensure the safety and efficacy of 3D printed dosage forms formulated with amorphous solid dispersion (Kim et al., 2021; Skowyra et al., 2015; Zhao et al., 2022).

Felodipine (FEL) is a class II hydrophobic drug in the Biopharmaceutics Classification System, with a poor water solubility of 0.58 μg/mL at 25° C, a melting point of 145 °C at crystalline state and a glass transition temperature (Tg) of 47 °C at amorphous state (Karavas et al., 2006; Lu et al., 2019). ASD technology has emerged as a promising strategy to improve the solubility and dissolution rate of felodipine (FEL) (Lu et al., 2019; Marsac et al., 2009, 2006; Palazi et al., 2018; Vo et al., 2017; Yi et al., 2019). In conjunction with this technique, GDDS can be used to improve drug release and absorption by maintaining a low concentration around the dosage forms, avoiding in situ recrystallization and allowing gradual drug absorption. GDDS have the ability to maximize the absorption area of drug molecules on the surface of the gastrointestinal tract, ensuring optimal absorption. In contrast, conventional controlled-release pharmaceutical forms can rapidly pass through the small intestine, which restricts their effectiveness (H. Blaesi and Saka, 2024; Vo et al., 2017).

The aim of this work was to manufacture FDM 3D printed (3DP) floating tablets composed of an ASD of felodipine with a hydrophilic polymer. For this purpose, the polymer Affinisol™ 15 LV (AFF) has been used as the carrier. Theoretical methods were employed to predict the drug-polymer interactions. Subsequently, the drug-loaded filaments and the 3DP tablets were studied using different analytical techniques for physical characterization and to complement the modeling predictions of the drug-excipient interactions. In addition, the buoyancy and release kinetics of the 3DP tablets were studied.

2. Materials and methods

2.1. Materials

Felodipine (Carbosynth Ltd., Compton, Berkshire, UK) was used as the model drug. Hydroxypropyl methylcellulose (HPMC) Affinisol™ 15 LV, a hydrophilic, amorphous polymer, was kindly donated by The Dow Chemical Company (Midland, MI, USA).

2.2. Methods

2.2.1. Preparation of physical mixtures

The binary physical mixtures used for the extrusion process were made by weighing out the samples. Previously, felodipine powder was sieved, and the size fraction used was smaller than 180 μm. The raw materials were manually mixed by a "geometric dilution" protocol. A mortar and a pestle were used until the homogenous physical mixtures were obtained. Physical mixtures contained 5, 10, and 15 % (w/w for these and following percentages) of FEL. The drug loading of 5 %, 10 % and 15 % were selected to obtain filaments for printing systems with therapeutic doses of felodipine (2.5–10 mg) as the target dose. The physical mixtures were placed in a vacuum desiccator for 24 h prior to extrusion.

2.2.2. Extrusion process

The mixtures were extruded using a twin-screw filament extruder ZE 9 (Three-Tec, Seon, Switzerland) to obtain the drug-loaded filaments. The extruder was operated at 33 rpm, extruding batches of around 5 g of the mixtures at 150 °C through a die with a diameter of 1.75 mm. To establish a thermal equilibrium before processing, the extruder's heat soak time was set to 15 min. The extruded filaments were stored in suitable packaging to avoid water uptake until printing.

2.2.3. Tablet design and 3D printing

The design of the 3D printed tablets was created using BlocksCAD software V1.13.0 (BlocksCAD, Burlington, MA, USA), exported as a stereolithographic (.stl) file and sliced on IdeaMaker V3.1.7 software (Raise3D Technologies, Irvine, CA, USA). The drug-loaded filaments were printed by FDM technique using a Pro2 Dual Extruder Raise3D printer (Raise3D Technologies, Irvine, CA, USA). The size of the cylindrical 3D printed tablets was 2.5 mm height x 7.5 mm width for the filaments containing 5 %, 10 %, and 15 % of FEL, based on the therapeutical doses of felodipine (2.5–10 mg) as the target dose for our 3DP tablets (Alhijjaj et al., 2016; Chaturvedi et al., 2014; Ghamami et al., 2014; Govender et al., 2021; Vo et al., 2017; Yi et al., 2019). Additionally, filaments containing 5 % of drug were selected to print tablets of 4 mm height x 10 mm width, to maintain therapeutic doses. The selected range of drug loading on the filaments allows the effects of drug loading and tablet size to be studied while maintaining therapeutic doses. The printing settings were as follows: nozzle diameter of 0.5 mm, nozzle temperature 200 °C, build plate temperature 80 °C, first layer height 0.2 mm, layer height 0.1 mm, printing speed of 10 mm/s, flow-rate 150 %, infill of 25 %, 1 sealing perimeter, 3 solid bottom layers and 4 solid top layers.

2.2.4. Characterization of the tablets

To assess the uniformity and reproducibility of the 3D printing process, the dimensions (height and diameter) and weights of the 3D printed tablets (n = 6) were determined using an electronic micrometer (Comecta, SA, Barcelona, Spain) and an analytical balance (Shimadzu AUW120, Manila, Philippines).

According to the European Pharmacopoeia, a hardness tester (Sotax HT1, Teknokroma, Spain) was used to assess the tablet crushing force (n = 6). Subsequently, the tablet tensile strength, σ_t, was calculated according to eq 1:

$$\sigma t = 2F/\pi dh \quad (1)$$

where F is diametrical crushing force (N), d is tablet diameter (mm), and h is tablet height (mm).

2.2.5. Evaluation of amorphous solid dispersion

- **Molecular Modeling**

The molecular dynamics simulations (MD) were conducted using YASARA software version 20.12.24 (YASARA Biosciences GmbH, Vienna, Austria) (Krieger and Vriend, 2014). Accelerated calculations were making use of graphic processing units (GPUs) to determine non-bonded interactions (Van der Waals and real-space Coulomb forces) (Krieger and Vriend, 2014). A general AMBER-type force field GLYCAM06 (Kirschner et al., 2008) and GAFF2 were employed (Wang et al., 2004), wherein atomic charges were based on a semi-empirical quantum chemical estimation (AM1BCC) (Jakalian et al., 2002).

A simplified HPMC as octamer was prepared in simulation box of 65x 65x 65 Å with randomly placed felodipine molecules corresponding to a concentration of 15 % (w/w) to match the experiments of the binary mixture. Following steepest decent and simulated annealing minimizations to remove clashes, a simulation run was conducted under periodic boundary conditions at 423 K for 15 ns to simulate an extrusion process. The second main simulation run was then conducted at 298 K (under periodic boundary conditions) and lasted another 15 ns. Equations of motion were integrated with a 2x 1 fs, which meant that intramolecular forces were calculated every 1 fs, while intermolecular forces were calculated every 2 fs to provide a full simulation step.

An NTP ensemble was used, where pressure control was achieved by rescaling the simulation cell along the x, y, and z axes to reach a constant pressure of 1 bar. For temperature control, atom velocities were rescaled using a weakly coupling thermostat that kept the macroscopic temperature at the requested value. The software did not use the strongly fluctuating instantaneous microscopic temperature to rescale velocities at each simulation step (i.e., a classical Berendsen thermostat) but instead, a scaling factor was calculated according to Berendsen's formula from the time average temperature to avoid artifacts occasionally observed with a classical Berendsen thermostat. A cut-off value of 8 Å was selected for the Van der Waals forces, and the particle mesh Ewald algorithm was applied to electrostatic forces (Essmann et al., 1995).

Finally, the interactions were calculated in 200 ps step (NTP ensemble) following the 15 ns equilibration at 298 K, and mean values from 10 sampling points were used for hydrogen bonding and hydrophobic interaction energy. The entire simulation runs were repeated with n = 4.

- **Surface area**

The determination of specific surface area employed the standard BET (Brunauer, Emmett, Teller) method using a Gemini VII 2390 Surface Area and Porosity Analyzer (Micromeritics Instrument Corporation, Norcross, GA, USA). The measurements were conducted at a relative pressure (p/p_0) within the range of 0.05–0.3. Prior to analysis, approximately 1200 mg of the samples were heated to 80 °C and kept for 24 h under a nitrogen atmosphere using the FlowPrep 060 instrument (Micromeritics Instrument Corporation, Norcross, GA, USA). The specific surface area of each sample was measured three times, and the mean values, as well as standard deviations, were calculated. Pure felodipine samples included particles of size > 180 μm. Drug-loaded filament samples were previously cryomilled and sieved, using a particle size > 250 μm for the cryomilled filament samples.

The specific surface area data were needed to evaluate the following gas chromatographic experiments. The surface area mean values and standard deviations of physical mixture and cryomilled filament of 15 % FEL were 0.045 ± 0.014 m^2/g and 0.078 ± 0.007 m^2/g, respectively.

- **Inverse Gas Chromatography**

Inverse Gas Chromatography (IGC) was conducted using a SEA-Surface Analyzer (Surface Measurement Systems Ltd., Wembley, United Kingdom) to characterize surface energies of the samples. IGC is based on the adsorption of a vapor (probe molecule) with known physicochemical properties onto a stationary adsorbent for analysis. A practically infinite gas dilution is hereby targeted for subsequent calculations of the surface energy. Approximately 1.2 to 1.7 g of each sample was inserted into a silanized column with a 4 mm internal diameter. To fix the powdery sample, silanized glass wool was plugged at both ends of the column. Prior to analysis, each column was conditioned at 30 °C for 2 h at 0 % RH with helium as a carrier gas at 10 standard cubic centimeters per minute (sccm). This procedure facilitated the removal of any moisture uptake or impurities from the system. Moreover, the dead volume was determined by methane injection before and after the main experiments at 30 °C (303 K). The gas injections targeted a 5 % nominal surface coverage (in proximity to the Henry region), and analytics was based on a flame ionization detector (FID). Besides the sample weight, the measured BET-specific surface areas were necessary for the targeted injection concentrations. The net retention volumes (V_N) were then determined using the respective peak center of mass (Peak CoM). The principle of iGC is based on injecting various organic probe solvents with known characteristics into the flow of the carrier gas. The extent of interactions between the solid phase of interest and the probe gas is determined by the net retention volume V_N (see eq 1):

$$V_N = \frac{j}{m} F(t_R - t_0)\frac{T}{273.15} \quad (2)$$

where T is the column temperature, F is the carrier gas flow rate at 1 atm and 273.15 K, m is the sample mass, t_R is the retention time of the absorbed probe gas, t_0 is the mobile phase hold-up time, and finally, j represents the James − Martin correction (that adjusts retention time for the pressure drop effect in the column bed). A free adsorption/desorption energy is then obtained by eq 2:

$$\Delta G = RTln(V_N) + K \quad (3)$$

where R is the gas constant and K is an experimental constant (Mohammadi-Jam and Waters, 2014). This total free energy is the sum of the dispersive and specific (acid − base) components of the free energy of adsorption (see eq 3) (Balard et al., 2000).

$$\Delta G_{total} = \Delta G_{dispersive} + \Delta G_{specific} \quad (4)$$

The dispersive surface energy was determined by a homologous series of n-alkanes (heptane, hexane, octane, and nonane), and the polar solvents dichloromethane, ethyl acetate, ethanol, acetone, and toluene were used for the determination of the specific part of the surface energy. The software Cirrus Plus (version 1.2.3.2 Surface Measurement Systems Ltd. (Wembley, United Kingdom)) was used for these energy calculations by selecting the "Della Volpe" scaling option and "Schultz" method for which more details can be inferred from the literature (Mohammadi-Jam and Waters, 2014). Measuring conditions were the same as applied

for sample conditioning and mean values and standard deviations are shown from duplicate measurements of three individual packed columns for each material.

- **Atomic Force Microscopy (AFM) and Laser Scanning Microscopy (LSM)**

Samples for AFM and LSM were previously cut and broken into small pieces. The AFM and LSM were performed at the Nano Imaging Lab in Basel, Switzerland.

Atomic force microscopy (AFM) images were taken in the oscillation mode keeping the amplitude constant (AC tapping mode) using a NanoWizard 4 AFM instrument (JPK Instruments AG, Berlin, Germany). Height and phase images were collected simultaneously using a 160AC-NA cantilever (Nanosensors AG, Neuchatel, Switzerland) with a resonance frequency of approximately 320 kHz and 26 Nm − 1 spring constant. The resolution of the images was 512 pixels per line.

Laser scanning micrographs of the sample surfaces were collected by means of a 3D laser scanning confocal microscopy (LSM) VK-X1100 (Keyence, Osaka, Japan) using a violet laser (408 nm) and a 150x objective lens (Nikon Plan CF Apo, 150x/0.95, WD 0.2 mm). The surface was scanned at high speed in X, Y and Z, allowing image capturing and height measurements with high lateral resolution. Reflected white light and laser light emitted from the focal point were reflected back through the objective lens. The intensity of the laser light that passes through a pinhole is determined by a very sensitive 16-bit photomultiplier. Since the pinhole blocks most of the returning light (except the light from the focal point), confocal LSM delivers much sharper images than conventional microscopy techniques. In addition, a true color image from the integrated second light source is overlaid.

- **Differential Scanning Calorimetry (DSC)**

Differential Scanning Calorimetry (DSC) was employed to investigate the thermal characteristics of the samples, and to confirm the compatibility between the drug and the polymer. A DSC 3 STARe system (Mettler Toledo, Greifensee, Switzerland) and a DSC Q20 V24.11 Build 124 were used for samples (about 5–12 mg) weighed into 40 μL aluminum pans covered with pierced aluminum lids. Nitrogen was set to 200 mL/min as the purge gas. The samples were heated at a ramp rate of 5 °C/min. Heating and cooling ramps at 10 °C/min rate were also used to find the glass transition temperature (T_g) of the samples. The temperature range was set from 40 to 280 °C. The thermograms were evaluated using the STARe Evaluation-Software version 16, and the TA Instruments Universal Analysis V4.7A, at the Functional Characterization Service of the CITIUS in the University of Seville.

- **X-ray Powder Diffraction (XRPD)**

The crystallinity of the samples was studied using a D2 Phaser diffractometer and a D8 Advance A25 diffractometer from Bruker AXS Ltd. (Karlsruhe, Germany), equipped with a copper tube anode (30 kV, 10 mA and 40 kV, 30 mA, respectively) and a Lynxeye® detector. The samples were automatically rotated at 15 rpm on a sample holder. The increment, number of steps, time per step and range 2θ range were set to 0.02°, 2124 steps, 1.5 s, and 6–40°, respectively. A filter of 0.02 Ni, a divergence slit scanning range of 0.5° (from 3° to 70° on a 2θ scale), and a scanning rate of 9°/min were set to the D8 Advance A25 diffractometer. The data were analyzed using DIFFRAC.SUITE EVA V7.3.1 software and DIFFRAC.SUITE EVA V5.2 software.

- **X-ray tomography**

X-ray tomography was performed using a Zeiss Xradia 610 Versa (Zeiss, Oberkochen, Germany) by the X-ray Laboratory Service of the CITIUS in the University of Seville, to evaluate the inner structure of the 3D printed tablets. The scan was conducted using no filter, at a peak voltage of 40 kV, using an optical magnification of 0.4X, and a pixel size of 0.88 μm. Reconstructor Scout-and-Scan v.16.0, 11, 592 software was used to perform the image reconstruction The images were exported as a 16-bit tiff file for visualization.

- **Scanning Electron Microscopy (SEM)**

The surface and inner portions of the samples were evaluated using Scanning Electron Microscopy (SEM) performed at the Microscopy Service of the CITIUS in the University of Seville with a FEI TENEO electronic microscope (FEI Company, Hillsboro, OR, USA) at 5 kV. Previously, a Leica EM SCD500 high vacuum sputter coater was used to apply a 10 nm-thin layer of Pt onto the samples.

2.2.6. *In vitro release studies*

Drug release studies of the 3D printed tablets were carried out on the Agilent 708-DS (Agilent, CA, USA) using 900 mL of a pH 1.2 HCl dissolution medium at 37 ± 0.5 °C, to simulate gastric conditions. 1 % sodium dodecyl sulphate (SDS) was added to the dissolution medium to ensure sink conditions, as previously reported (Brown et al., 2004; Mahmah et al., 2014; McDonagh et al., 2023; Vo et al., 2017). The study was performed in a basket apparatus in triplicate for each batch during 24 h at 50 rpm. The basket apparatus is better suited for preventing erosion of the surfaces of swelling hydrophilic tablets compared to the paddles. The buoyancy was also evaluated through the drug release studies, studying the float lag time and the overall duration of floating. The percentage of drug released was analyzed using a UV–vis spectrophotometer Agilent 8453 (Agilent, CA, USA) at a wavelength of 363 nm (Nimje et al., 2011).

The drug release kinetics were also investigated according to Zero order (4), Higuchi (5), Korsmeyer (6) equations (Higuchi, 1963; Korsmeyer et al., 1983):

$$(Mt/M\infty) = k_0 \cdot t \tag{4}$$

$$(Mt/M\infty) = k \cdot t^{0.5} \tag{5}$$

$$(Mt/M\infty) = k_K \cdot t^n \tag{6}$$

where M_t/M_∞ is the fractional drug release at time t (drug loading is considered as $M\infty$); k is the Higuchi kinetic constant. k_K is the Korsmeyer's kinetic constant, t is the release time, n is a release exponent that depends on the release mechanism and the shape of the system (Ritger and Peppas, 1987). Finally, k_0 is the zero-order release rate constant.

2.2.7. *Statistical analysis*

The data are expressed as mean ± standard deviation (SD). Statistical analysis was performed using IBM SPSS Statistics Software (Version 26), by one-way analysis of variance (ANOVA), followed by Scheffe's post-hoc test. This analysis aimed to discern variations in drug release profiles attributable to the considered formulation factors, namely, drug load and the size of the 3D printed tablet. The significance level was determined at a 95 % confidence limit, with factors demonstrating $p \leq 0.05$ deemed as statistically significant.

3. Results and discussion

3DP technology has gained much attention in the pharmaceutical sciences based on the potential to obtain patient-centric dosage forms that are tailored to individual medical needs. Due to the biopharmaceutical challenges associated with especially poorly water-soluble drugs, a combination of ASD and 3DP technology has become a topic of interest (Ayyoubi et al., 2021; Gala et al., 2020; Patil et al., 2016). In this study, formulations of FEL and AFF were developed to produce drug-loaded filaments through HME, which were then utilized in FDM

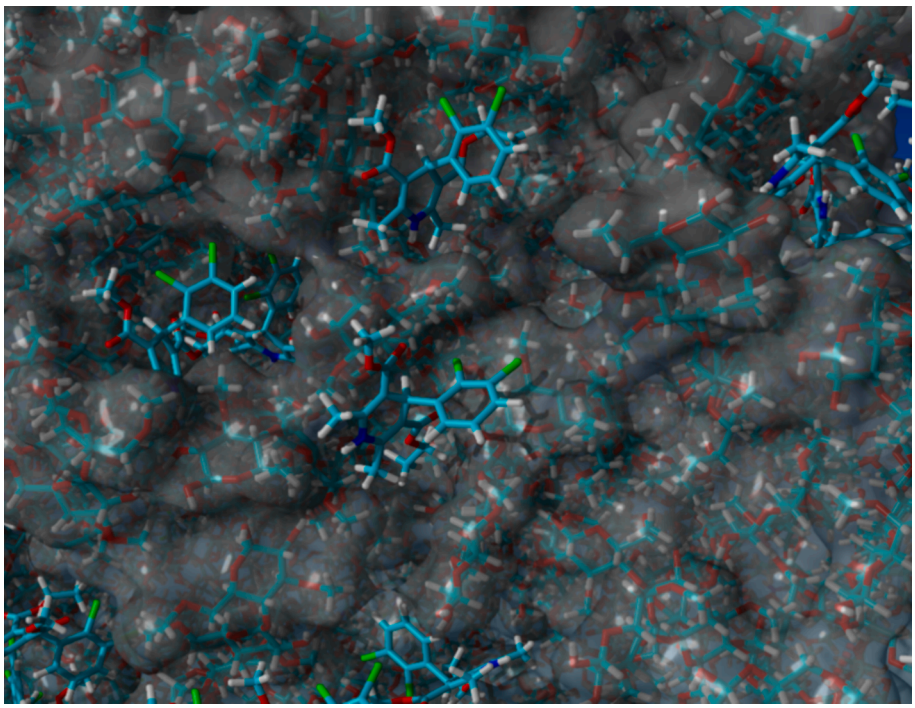

Fig. 1. Snapshot of a molecular dynamics (MD) simulation (after the cycle at 298 K, 15 ns) with felodipine and HPMC as tube model, where for the latter polymer, a semi-transparent molecular surface area is shown.

3DP technology, with the aim of obtaining ASDs. In the manufacturing process, different steps were followed to ensure and evaluate the formation of ASDs. This evaluation consisting of two phases (theoretical and experimental studies) will reduce resource consumption and increase accuracy in optimizing a 3D printing process, and by extension, formulation, extrusion process, and final printed systems (Censi et al., 2018; Thakkar et al., 2020). For the theoretical study, solubility parameter estimation and molecular simulations were employed. On the experimental side, different bulk and surface analytics were conducted to physically characterize the obtained mixtures.

HPMC AFF was used as the polymeric carrier, as HPMC grades are common hydrophilic polymers utilized in stabilizing amorphous solid dispersions. HPMC is widely used in extended-release systems (Aho et al., 2017; Mandal et al., 2016; Notario-Pérez et al., 2018; Reynolds et al., 2002; Yi et al., 2019; Zhang et al., 2017). Moreover, cellulose derivatives such as HPMC are well known for their low toxicity (Select Committee on GRAS Substances (SCOGS), 1973). Affinisol™ 15LV is a modified HPMC polymer designed by Dow Chemical Company for utilization in HME applications. In addition, this polymer has shown good printability properties without additives (Gupta et al., 2016; Mašková et al., 2020; Prasad et al., 2019).

3.1. Theoretical approach for the evaluation of ASD

3.1.1. Solubility parameter

Firstly, the miscibility of the FEL and AFF was studied. It is crucial to know the solubility/miscibility of drugs in polymers when developing ASDs. This knowledge provides useful information regarding prediction of the stability of solid dispersions (Greenhalgh et al., 1999; Lu et al., 2016; Page et al., 2016). Thus, close solubility parameter values of the mixture components mean that the cohesive energy between the drug and excipient(s) matches, which is a viable method to initially estimate the miscibility of the drug and matrix (Jankovic et al., 2019; Thakkar et al., 2020).

Therefore, two substances are known to show good miscibility when the difference in their solubility parameters is less than 7 $MPa^{1/2}$, especially when this difference is less than 2 $MPa^{1/2}$ (Greenhalgh et al., 1999); whereas the substances are not considered miscible when the difference is larger than 10 $MPa^{1/2}$. According to the literature, the solubility parameter is 22.7 $MPa^{1/2}$ for FEL (Lu et al., 2016) and 24.0 $MPa^{1/2}$ for HPMC (Newman, 2015) according to the Hoftyzer/Van Krevelen method calculations (Van Krevelen and Te Nijenhuis, 2009). Therefore, the solubility parameters of FEL and AFF are very close to each other, which indicates a good miscibility of drug–polymer.

3.1.2. Molecular simulations

The molecular modeling showed, following the simulated extrusion and subsequent equilibration cycle at room temperature, that felodipine was dispersed in the polymeric matrix without forming aggregated clusters, which could have otherwise pointed to a possible phase separation (see Fig. 1). This result was in line with the previously discussed consideration of solubility parameters in that felodipine was well dispersed in the HPMC carrier. Despite this molecular-level dispersion, there was still not an entirely uniform distribution of the drug in the matrix noted because some surface accumulation of felodipine was noted. This finding agreed with previous molecular dynamics (MD) simulations using a simulated annealing protocol where ibuprofen molecules were observed to stick out of polymeric coils in the solid dispersions (Ouyang, 2012).

Regarding the molecular interactions, there was a notable contribution of hydrogen bonding energy that was on the average 40.2 %, whereas the remaining 59.8 % of the total interaction energy was due to hydrophobic interactions. The mean value of the ratio of total hydrophobic to H-bonding interaction energy was 1.5. The individual hydrophobic contacts were only 0.75 to 0.76 kJ per contact but appeared in great numbers as in these long-range interactions. Therefore, the net molecular drug-polymer interaction was more impacted by these Van der Waals forces than hydrogen bonding although individual hydrogen bonds were found to have on the average 19 kJ per bond. The drug was more accepting hydrogen bonds than donating, which was expected from the chemical structure of felodipine. Thus, the compound possesses a hydrogen bond donor N–H group and two hydrogen bond acceptor groups from the ester moieties that enter hydrogen bonding with HPMC.

In summary, the simulation results indicated a molecular-level

Table 1
Means and standard deviations values (n = 3) of the dispersive, specific, and total surface energy of physical mixture and filament (15 % of FEL) obtained from the IGC experiment.

Sample name	Mean dispersive surface energy (mJ/m^2)	Mean specific surface energy (mJ/m^2)	Mean total surface energy (mJ/m^2)
Physical mixture	18.8 ± 2.1	12.8 ± 0.9	31.6 ± 3.0
Cryomilled filament	23.1 ± 0.9	14.1 ± 0.2	37.2 ± 1.0

distribution of the drug in the HPMC matrix, which was partly due to strong excipient interactions from both hydrophobic as well as hydrogen bonding interactions that collectively suggested good miscibility. The present findings are overall in good qualitative agreement with previous work on felodipine where the effect of water was studied, which indicated the tendency that hydrogen interactions being favorable to miscibility with the cellulosic polymer were partly disrupted in presence of water (Xiang and Anderson, 2017). Therefore, the good miscibility as indicated by the MD simulations could be potentially hampered by substantial water-uptake at relatively higher humidity conditions.

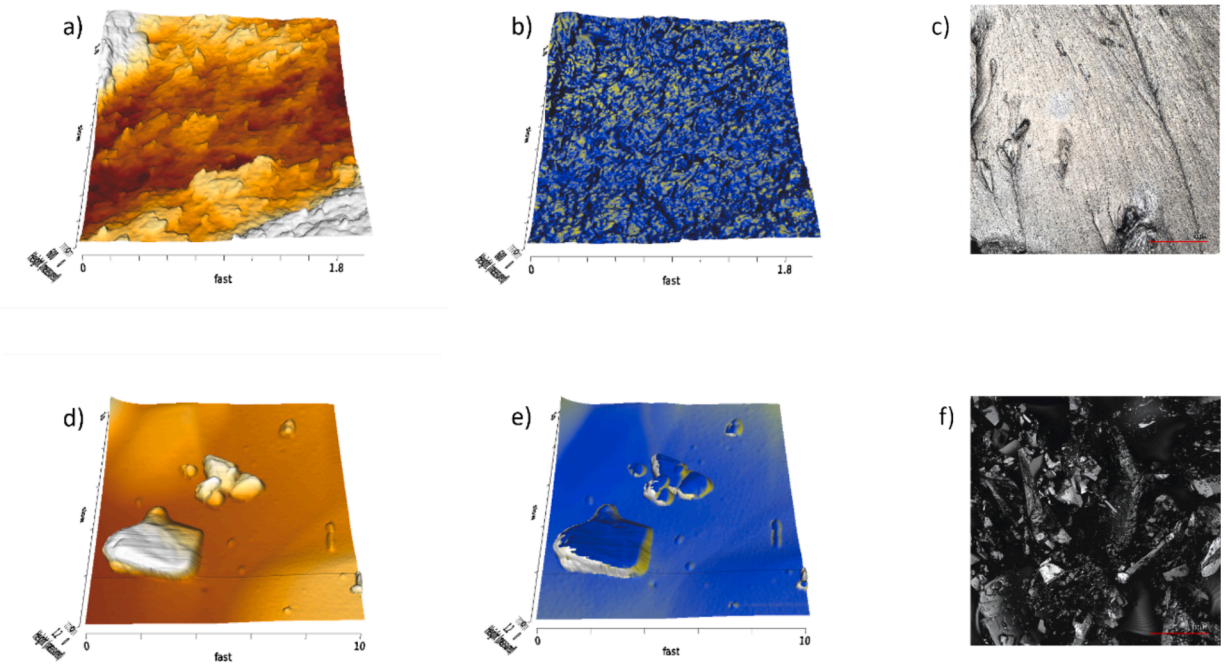

Fig. 2. Images of the drug-loaded filaments containing 15% of felodipine (a) AFM topographical, (b) 3D-overlaid height/phase, and (c) confocal LSM; images of powder felodipine (d) AFM topographical, (e) 3D-overlaid height/phase, and f) LSM.

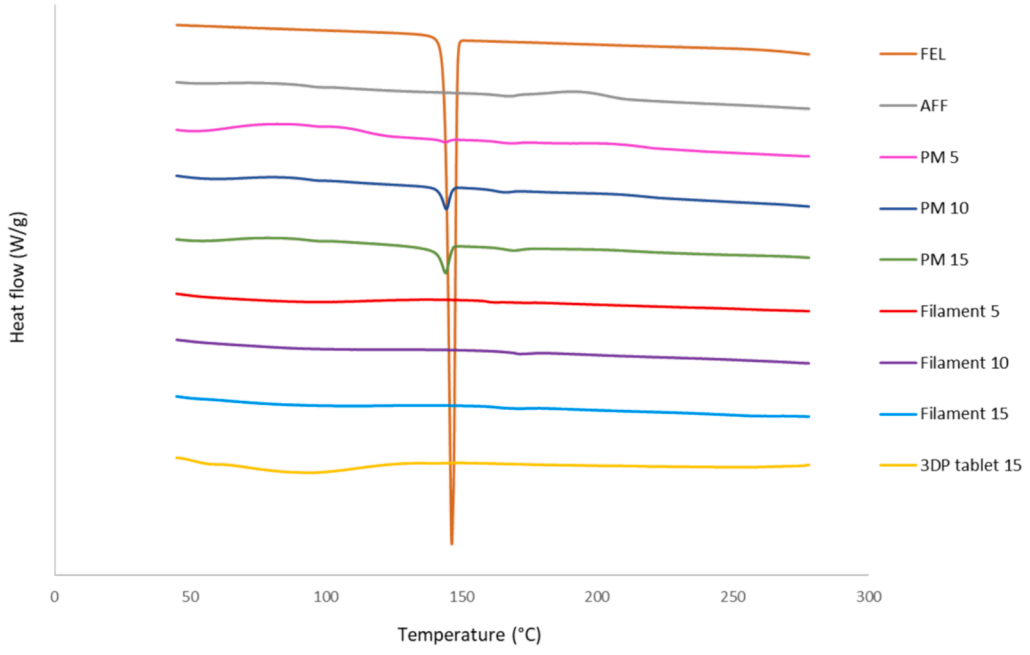

Fig. 3. DSC thermograms of FEL, AFF, the physical mixture (PM 5, PM 10, PM15), extruded filament with 5%, 10%, and 15% drug loading and 3DP tablet with 15% drug loading.

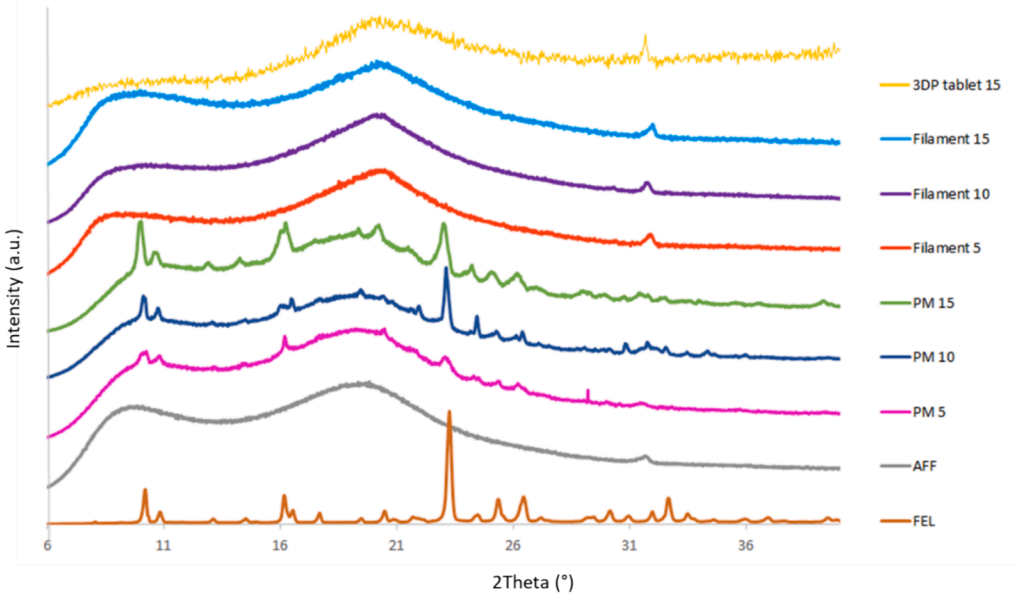

Fig. 4. XRPD patterns of FEL, AFF, the physical mixtures (PM 5, PM 10, PM15), extruded filament with 5%, 10%, and 15% drug loading and 3DP tablet with 15% drug loading.

3.2. Experimental approach in evaluating ASD

As the theoretical studies have shown positive results concerning solubility and potential for interactions leading to the formation of stable ASDs, the experimental phase was carried out.

3.2.1. IGC analysis

The IGC analysis was used to obtain measurements for dispersive, specific, and total surface energy, as detailed in Table 1. In this work, IGC analysis was applied for the first time to extrudates, suggesting this analysis as part of the experimental approach to evaluate ASDs.

Regarding the dispersive surface energy, higher values signify increased hydrophobic interactions, while a higher specific surface energy indicates the prevalence of hydrogen bonding interactions (Mohammadi-Jam and Waters, 2014; Voelkel et al., 2009). As shown in Table 1, both the physical mixture and the cryomilled filament exhibit dispersive surface energies that exceed their specific surface energy. The data reveal that 59.5 % of the total surface energy comes from hydrophobic interactions, while the remaining 40.5 % is attributed to hydrogen bonding interactions, for the physical mixture. The dispersive surface energy was higher for the filament than for the physical mixture. In this case, 62.1 % of the total surface energy comes from hydrophobic interactions, while the remaining 37.9 % is attributed to hydrogen bonding interactions. These findings of the combination of hydrogen bonding and hydrophobic interactions validate the predictions of the MD simulation.

3.2.2. AFM and LSM analysis

AFM can be used to evaluate the drug-polymer miscibility, residual crystalline drug, phase separation and recrystallization (Alzahrani et al., 2022; Censi et al., 2018; Ditzinger et al., 2019; Saboo et al., 2021). AFM was employed in this work for detecting residual felodipine crystals within the amorphous solid dispersion. Samples of drug-loaded filament containing 15 % of FEL (the higher drug-load used in this work) and pure felodipine were analyzed. The representative images are visible in Fig. 2. As can be observed, crystalline areas cannot be distinguished in Fig. 2(a), nor in 2(c), where the sample is shown as a homogeneous matrix. Furthermore, as MD simulation results predicted, a phase separation cannot be detected in Fig. 2(b). Drug-loaded filament is shown as a continuous matrix (Fig. 2a-c). Fig. 2d-f illustrate the morphology of pure felodipine crystals within a powdered felodipine sample. Thus, these results confirm the formation of an amorphous solid dispersion between AFF and FEL through the extrusion process.

3.2.3. Thermal characterization

DSC studies were performed to evaluate the physical state of FEL in the different steps of the manufacturing process. The thermal behavior of pure substances, physical mixtures, drug-loaded filaments, and 3D printed tablets is presented in Fig. 3.

The DSC results showed that pure felodipine exhibited a sharp endothermic peak at 147 °C, which was a melting peak (Yi et al., 2019). This demonstrated the crystallinity of the drug. This peak can be also observed in the physical mixtures' samples. However, this peak was no longer evident in drug-loaded filaments and 3D printed tablet samples. The absence of the melting point at this temperature in the thermographs of filaments and 3DP tablet, indicates that the drug is in amorphous state (Parulski et al., 2022). Regarding the degradation of the drug, no felodipine degradation event was observed in the felodipine thermogram or in the physical mixtures, filaments and 3DP tablet thermograms, which agrees with other works that reported that the degradation temperature of felodipine was higher than 230 °C (Alhijjaj et al., 2016; Govender et al., 2020; Guo et al., 2020). This would mean that no degradation of the drug would occur during the extrusion and printing processes. Moreover, it can be observed a T_g at 167 °C in the samples of filament and 3DP tablet containing 15 % of FEL (Fig. S1 in Supplementary material). Thus, this suggested that amorphous solid dispersions of FEL and AFF were indeed obtained from the formulations used in this work, through the extrusion and 3D printing processes. AFF has demonstrated to be a suitable polymer to form ASD with felodipine but also with other drugs, such itraconazole as it was shown in a previous study (Parulski et al., 2022).

3.2.4. X-ray powder diffraction (XRPD)

X-ray powder diffraction patterns of the pure substances, physical mixtures, drug-loaded filaments, and 3D printed tablet were collected (Fig. 4) to qualitatively examine the changes in the physical state of the materials.

The XRPD pattern of AFF did not show intensity diffraction peaks suggesting amorphous samples (Solanki et al., 2018). In contrast, the XRPD pattern of pure felodipine exhibited sharp 2θ diffraction peaks at

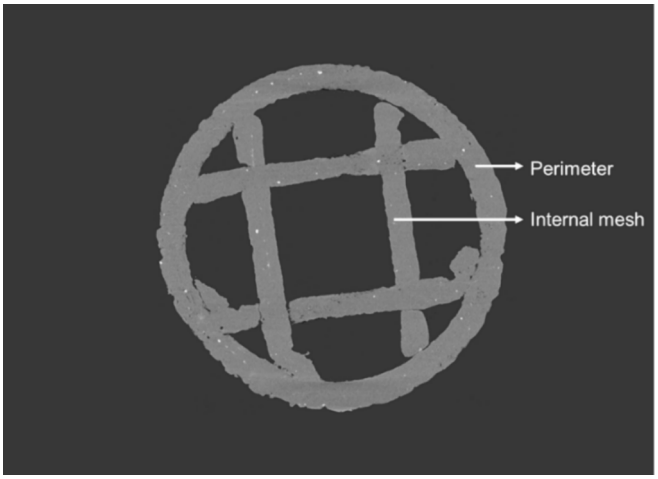

Fig. 5. A cross-sectional top view X-ray tomography image of the strands of the 3DP tablet. Arrows indicate the perimeter and the internal mesh of the tablet.

0.20°, 16.15°, 23.24°, 23.33°, 26.43°, 32.65°, confirming the crystallinity of the drug. As it can be observed in Fig. 4, the pattern of the physical mixtures showed the characteristics peaks of FEL. However, the XRPD patterns of the filaments and 3D printed tablet did not show diffractions peaks, confirming the complete amorphization of the FEL with AFF during the extrusion and 3D printing processes, in agreement with the DSC results (Fig. 3). The peak at ca. 32° observed in the filaments and 3DP tablet belongs to AFF (polymer) as it can be seen in the AFF diffractogram.

Overall, the XRPD and DSC data corroborated the prediction by the solubility parameter and molecular modeling study and were also useful for assessing the state of the material in the different steps of manufacturing 3DP tablets. These techniques of evaluation of ASD (XRD and DSC) are the most frequently used in other works dealing with extrudates and 3DP systems (Alhijjaj et al., 2016; Govender et al., 2020; Ilyés et al., 2019; Solanki et al., 2018).

3.2.5. *X-ray tomography*

3D printed tablets containing 15 % of FEL were also analyzed by X-ray tomography images. Fig. 5 shows a cross-sectional top view X-ray tomography image of the strands of the tablets. The image shows the perimeter as well as the strands that form a quadrilateral internal mesh. As it can be seen, no crystals are detected given that the image shows a homogeneous matrix. This suggests that the strands of 15 % of FEL with AFF are still an amorphous solid dispersion in the 3D printed tablets. This confirmed the predictions that the formulation with the maximum drug content used in this work provided indeed an amorphous solid dispersion.

3.2.6. *SEM images*

Through SEM images, the surface of filaments and 3DP tablets was analyzed. As it can be observed in Fig. 6a-c, filaments present a smooth and homogeneous surface, with an absence of visible crystals. Again,

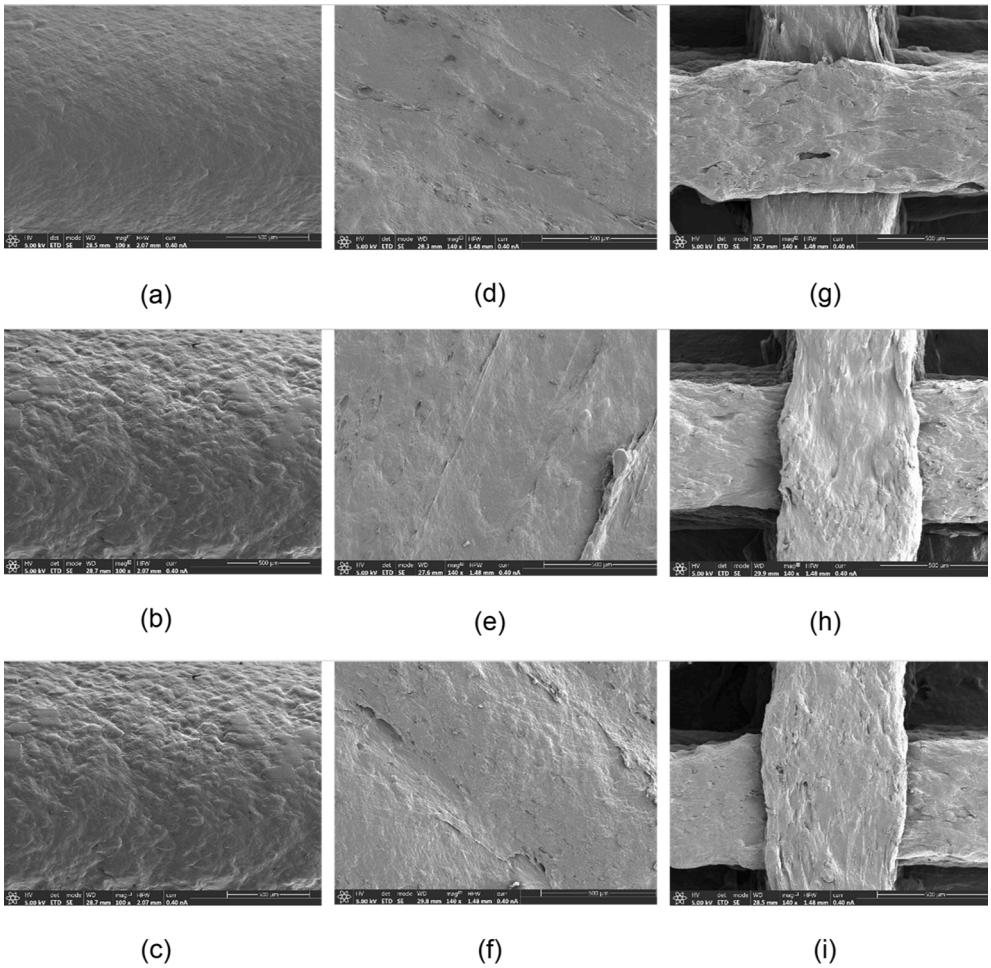

Fig. 6. Drug-loaded filaments surface from 5%, 10% and 15% of felodipine (a, b, c, respectively). Solid top layer of the 3DP tablets made with the filaments of 5%, 10% and 15% of felodipine (d, e, f, respectively). Internal mesh of the 3DP tablets made with the filaments of 5%, 10% and 15% of felodipine (g, h, i, respectively).

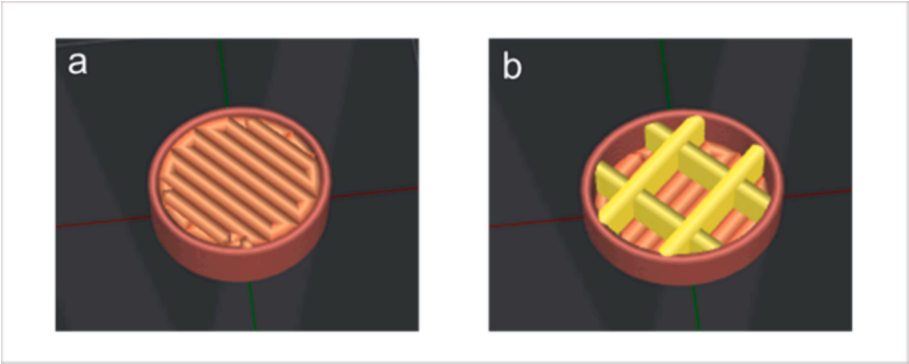

Fig. 7. Images of the digital design of the (a) top solid layer, (b) internal structure of the 3D printed tablet.

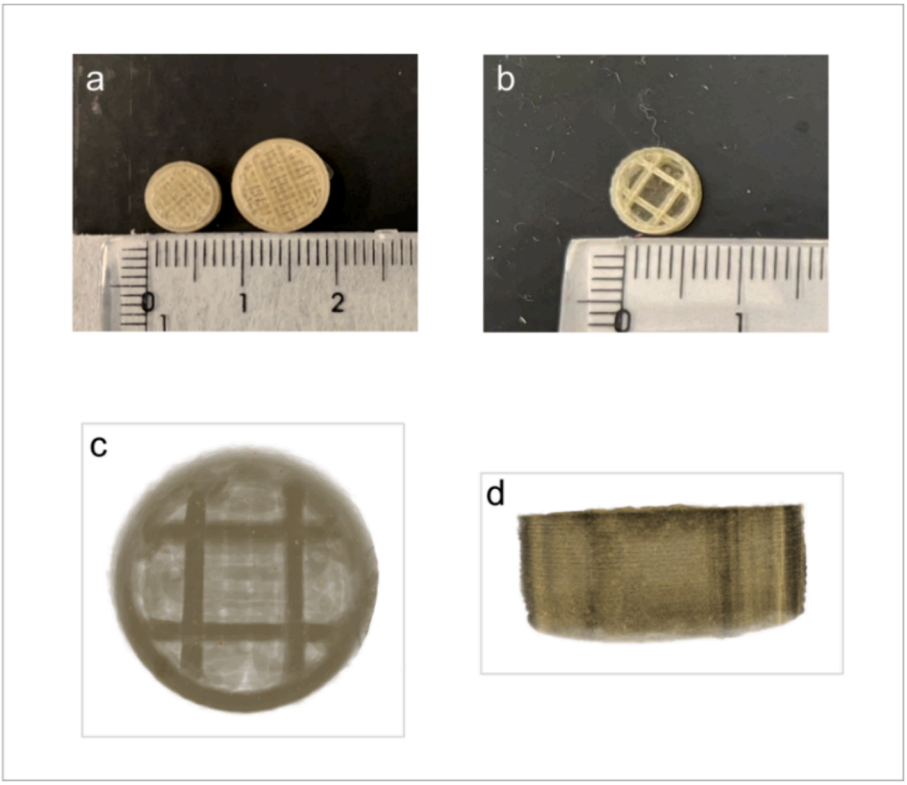

Fig. 8. Digital images of the 3D printed tablet: (a) top solid layer, (b) internal structure. X-ray tomography images of (c) top view of 3DP tablet; (d) external perimeter of 3DP tablet.

this confirmed again that an amorphous solid dispersion was obtained with the formulations used in this work.

As also occurred in the filaments, the SEM images of the 3DP tablets display homogeneous surfaces, both on the external surface (Fig. 6d-f) and internal mesh (g-i), confirming that the amorphous solid dispersion persists after the 3D printing process.

However, the long-term physical stability of ASD could be affected by the relative humidity (RH). The impact of RH on stability increases with the rising hydrophilicity of the pure polymers used in the formulations. Other works using felodipine reported that the formulations with felodipine and HPMCAS remained miscible even at 94 % RH. Felodipine crystallization rates from dispersions were found to be not very sensitive to changes in storage RH (Lehmkemper et al., 2017; Rumondor et al., 2009; Rumondor and Taylor, 2010). Additionally, felodipine was found to be a so-called class III compound regarding its recrystallisation tendency (Baird et al., 2010). Accordingly, the inherent recrystallisation tendency of felodipine is lower than with many other compounds, especially those that are in class II or even I (so-called "fast crystallizing compounds"). In view of the foregoing, the release data showed in Section 3.4 can be viewed as in good agreement with the inherent low recrystallisation nature of felodipine.

3.3. Physical appearance and characterization of 3D printed tablets

3D printed tablets were designed (Fig. 7) and extruded (Fig. 8) layer by layer by FDM, onto a build plate covered by blue tape, according to the digitally designed object. First, FDM extrudes solid underlayers. In our design, these underlayers consist of parallel filaments without any gaps, forming solid layers rather than a network structure. Above the solid bottom layers, parallel lines with gaps between them are built in perpendicular direction from one layer to the next one. Thus, a quadrilateral internal mesh was created. Finally, the FDM extruder formed the solid top layers to complete the object. All these steps were automatically performed, building the systems without the need for drying

Table 2
Physical characterization of the 3D printed tablets in two different sizes: A) 2.5 mm x 7.5 mm, B) 4 mm x 10 mm.

3DP Tablets	Weight (mg)	Height (mm)	Diameter (mm)	Density (g/mL)	Surface area (mm^2)	Surface area/Mass (mm^2/mg)
5A	99.15 ± 3.71	2.80 ± 0.08	7.56 ± 0.01	0.79 ± 0.02	156.57 ± 2.43	1.58 ± 0.04
10A	101.03 ± 3.4	2.75 ± 0.08	7.62 ± 0.12	0.80 ± 0.02	157.27 ± 5.94	1.56 ± 0.03
15A	96.5 ± 6.88	2.89 ± 0.07	7.46 ± 0.03	0.76 ± 0.06	155.42 ± 2.05	1.62 ± 0.12
5B	203.5 ± 2.78	3.79 ± 0.04	10.09 ± 0.04	0.67 ± 0.01	280.19 ± 0.79	1.38 ± 0.02

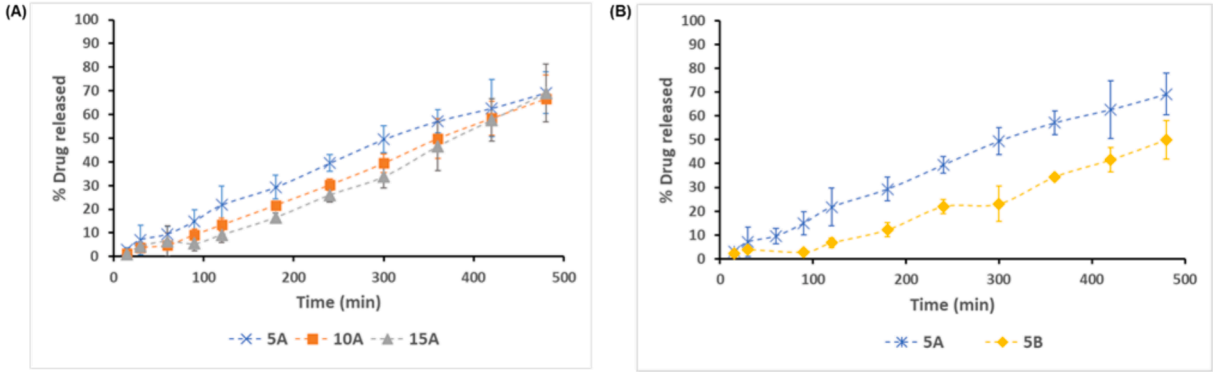

Fig. 9. In vitro drug release profile of 3D printed tablets (mean ± SD, n = 3): (A) Effect of the drug load, (B) Effect of the size of the 3D printed tablet on the drug release profiles.

steps. The internal mesh served as a support for the solid top layers. Hollow structures would otherwise have no support under the top of the tablets and could dent (Kimura et al., 2019).

Two different sizes of the 3DP tablets were prepared with the drug-loaded filament of 5 % FEL to obtain therapeutic dose of 5 and 10 mg (Fig. 8a): 2.5 mm height x 7.5 mm width, and 4 mm height x 10 mm width, respectively. The drug loaded filaments containing 10 % and 15 % of FEL were used to prepare 2.5 mm height x 7.5 mm width 3DP tablets. Images from Fig. 8b-d present the internal mesh, the solid top layer covering the inner part of the 3DP tablet as well as the sealing perimeter, showing the enclosed structure of the 3DP tablet, according to the 3D design.

3D printed tablets were successfully obtained using the drug-loaded filaments extruded in this work (containing 5 %, 10 % and 15 % of drug). The dimensions and weights of the systems were measured, and their densities, surface area, and surface area/mass ratio were calculated. Table 2 summarizes these results.

The resulting tablet dimensions were as expected based on the design of the tablets in the two different tablet sizes. In addition, although the weight of the bigger tablets was twice that of the smaller ones, the density values were similar, around 0.75 g/mL. Moreover, a force of 126.50 ± 18.19 N was detected by the hardness test for 15A tablets. Their tensile strength was 3.69 ± 0.53 N/mm^2.

3.4. Drug release behavior

The obtained 3DP tablets were placed in the dissolution medium for performing the dissolution tests. All of them floated from the beginning of the studies (floating lag time = 0 s). The systems kept floating during the entire drug release studies until they were completely dissolved. This buoyancy success can be attributed to the enclosed structures formed by the external perimeter and the solid top and bottom layers. This fact, coupled with the low infill percentage, enabled the tablets to retain air, facilitating their flotation.

For comparison, Parulski et al., 2022 prepared 3DP tablets, using AFF and itraconazole, with an open design (without solid top and bottom layers) while using an infill lower than 50 %. In these printed systems, the total drug release lasted less than 5 h (Parulski et al., 2022). However, due to the enclosed structure of our 3DP tablets with an infill of 25 %, a controlled drug release for more than 8 h was made possible (Fig. 9).

The study was performed in triplicate for each batch during 24 h. The drug content of the 3DP tablets was measured at the end of the dissolution test (after 24 h). The mean values of the drug released percentage of each batch were 100.60 %, 97.72 %, 99.99 % and 101.35 % for the batches 5A, 10A, 15A and 5B, respectively, after 24 h. Thus, felodipine was completely released after 24 h (Figure S2 in Supplementary material). The CV (%) values of the drug content for each batch were 3.61, 2.44, 4.61 and 6.25, respectively. Since the content variation for each batch was less than ± 15 %, according to Ph. Eur., the 3DP tablets meet the content uniformity criteria.

- Effect of drug load

The influence of drug load on the drug release behavior was studied in the in vitro dissolution tests (Fig. 9A). The dissolution studies were performed on tablets made of drug-loaded filaments containing 5 %, 10 % and 15 % FEL, keeping the size constant (2.5 mm height x 7.5 mm width). As shown in Fig. 9A, the drug release profiles of the three different drug-loads did not show significant differences. Varying the drug-load between 5 % and 15 % did not influence the drug release rate. Yi et al reported that the release profiles of felodipine, using hydrophilic polymers, were similar when the drug-load increased from 10 % to 40 % (Yi et al., 2019). This is also in agreement with our previous work, with metformin and AFF, where drug loads between 10 % and 20 % showed no influence on the release rate (Mora-Castaño et al., 2023).

- Effect of the size of the systems

The influence of the 3DP tablet size was also studied in the in vitro dissolution tests (Fig. 9B). 3D printed tablets with different sizes were made with the 5 % drug-loaded filament. Their drug release profiles are shown in Fig. 9B. As it can be observed, the smaller 3DP tablets (5A) −2.5 mm height x 7.5 mm width− presented a slower drug release rate than the bigger ones (5B) −4 mm height x 10 mm width−. The statistical analysis showed significant differences confirming that the size of the systems was a variable that influenced drug release behavior. The influence of the system size has also been reported before. Thus, a faster

Table 3
Mathematical modeling and drug release kinetics of 3D printed tablets: Higuchi kinetic constant (b); release exponent (n); determination coefficient (r^2); Korsmeyer kinetic constant (k_K).

3DP Tablets	Zero Order		Higuchi		Korsmeyer		
	K	r^2	b	r^2	k_K	n	r^2
5A	0.1556	0.9969	0.0362	0.9924	0.0022	0.9949	0.9949
10A	0.165	0.9988	0.0333	0.9828	0.0004	0.9998	0.9998
15A	0.1569	0.9909	0.0322	0.9635	0.0007	0.9519	0.9519
5B	0.1185	0.9977	0.0266	0.9861	0.0000	1.6242	0.9787

release profile was observed in smaller size 3DP tablets compared to that of bigger ones (Pietrzak et al., 2015; Skowyra et al., 2015). This is likely to be related to their larger surface area/mass ratio, as well as the smaller surface area (Pietrzak et al., 2015; Skowyra et al., 2015; Yi et al., 2019). The surface area/mass ratio of our tablets (see Table 2) was in agreement with this argument.

3.5. Drug release kinetics

Dissolution data were analyzed to elucidate the drug release mechanism of FEL from the 3D printed tablets. The dissolution data ($Mt/M\infty \leq 0.6$) were fitted to the zero-order, Higuchi and Korsmeyer equations. As Fig. 9 shows, two phases can be distinguished. The first phase covers the first 90 min. Initially, due to incomplete swelling of the polymer, the drug remained trapped within the inner part of the tablet. Water absorption was greater than diffusion outflow, thus impeding drug release from the whole matrix. Therefore, drug would be primarily released from the external part in direct contact with the release medium. Subsequently, the release medium would penetrate through the external and internal structural matrix so the drug release would occur from the whole system.

An additional explanation for this behavior could be the argument provided by Vo et al., 2017. These authors reported that, using FEL and hydrophilic polymers, the hydrated polymer formed a gel that is needed to release the drug from the whole matrix (Vo et al., 2017). If the polymer is not completely hydrated, the drug release would be limited, with a lower initial drug release rate as the polymer begins to hydrate.

The kinetic of the second phase of the drug release is studied in Table 3. The determination coefficients (r^2) showed that the drug release was best fitted to the zero-order model. Moreover, it should be highlighted that the n value on the Korsmeyer equation was higher than 0.89, approaching a zero-order kinetic (Sandoval et al., 2008). Drug release from the hydrated polymer can occur, as in the case of hydrophilic HPMC-based matrices, by diffusion or by erosion of the polymer (Ferrero et al., 2013; Yi et al., 2019). The value obtained for the Korsmeyer exponent suggests a combination of both mechanisms.

Furthermore, the values of the Korsmeyer constant, k_K, were close to zero, indicating that a burst release did not occur in our systems. Therefore, the kinetic study demonstrated that the intended zero-order release of the systems was indeed obtained. This also agreed with the straight lines of the drug release profiles (Fig. 9). Zero-order kinetic is deemed as ideal for all controlled release drug delivery systems, including gastroretentive systems, since as the drug release rate remains constant over the entire release duration, this typically facilitates constant drug levels in the plasma (Gokhale, 2014; Zhang et al., 2017; Zhao et al., 2017).

4. Conclusions

Combination of HME and 3DP can be viewed as a promising field in pharmaceutical additive manufacturing, but applied research is required to advance the technology to galenical practice. The present work initially used in silico tools for characterization of the intended amorphous solid dispersions by making use of solubility parameter estimation and full atomistic MD simulations. This initial digital evaluation constitutes a step forward in the amorphous solid dispersion formulation development for 3D printing technology in the pharmaceutical field. On the other hand, the combination of physical bulk and surface characterization methods used in this work provided a thorough analysis of pharmaceutical quality for both drug-loaded filaments and 3D printing tablets. Accordingly, the amorphous solid dispersions obtained with the binary formulations of FEL and AFF have demonstrated their robustness by remaining physically stable throughout the printing process. Finally, 3D printing emerges as a pharmaceutical technology to manufacture floating drug delivery systems. The design used in this work allowed to obtain low density systems. This resulted in buoyancy during the entire drug release process until a complete dissolution of the 3D printed tablets was attained. The particular design of the printed dosage form enabled with a single polymer to achieve a zero-order controlled drug release, which is considered the ideal kinetics for a gastroretentive system.

CRediT authorship contribution statement

Gloria Mora-Castaño: Writing – review & editing, Writing – original draft, Investigation, Formal analysis, Data curation, Conceptualization. **Mónica Millán-Jiménez:** Writing – review & editing, Writing – original draft, Supervision, Project administration, Investigation, Funding acquisition, Conceptualization. **Andreas Niederquell:** Writing – review & editing, Investigation, Formal analysis, Data curation. **Monica Schönenberger:** Writing – review & editing, Investigation, Data curation. **Fatemeh Shojaie:** Writing – original draft, Visualization. **Martin Kuentz:** Writing – review & editing, Writing – original draft, Supervision, Project administration, Conceptualization. **Isidoro Caraballo:** Writing – review & editing, Writing – original draft, Supervision, Project administration, Funding acquisition, Conceptualization.

Declaration of competing interest

The authors declare that they have no known competing financial interests or personal relationships that could have appeared to influence the work reported in this paper.

Data availability

The Authors enable the use of all the reasearch data

Acknowledgments

This work was supported by MCIN/AEI/10.13039/501100011033 and ERDF A way of making Europe (project RTI2018-095041-B-C31); Junta de Andalucía, Consejería de Economía, Conocimiento, Empresas y Universidad (project US-1380923); and Ministerio de Ciencia, Innovación y Universidades (grant number FPU18/05665 and EST22/00038). The authors thank María Dolores Domínguez Franco from Functional Characterization Service of the CITIUS in the Universidad de Sevilla for her contribution to this work.

Appendix A. Supplementary data

Supplementary data to this article can be found online at https://doi.org/10.1016/j.ijpharm.2024.124215.

References

Aho, J., Halme, A., Boetker, J., Water, J.J., Bohr, A., Sandler, N., Rantanen, J., Baldursdottir, S., 2017. The effect of HPMC and MC as pore formers on the rheology of the implant microenvironment and the drug release in vitro. Carbohydr. Polym. 177, 433–442. https://doi.org/10.1016/J.CARBPOL.2017.08.135.

Alhijjaj, M., Belton, P., Qi, S., 2016. An investigation into the use of polymer blends to improve the printability of and regulate drug release from pharmaceutical solid dispersions prepared via fused deposition modeling (FDM) 3D printing. Eur. J. Pharm. Biopharm. 108, 111–125. https://doi.org/10.1016/J.EJPB.2016.08.016.

Alzahrani, A., Nyavanandi, D., Mandati, P., Youssef, A.A.A., Narala, S., Bandari, S., Repka, M., 2022. A systematic and robust assessment of hot-melt extrusion-based amorphous solid dispersions: Theoretical prediction to practical implementation. Int. J. Pharm. 624, 121951 https://doi.org/10.1016/J.IJPHARM.2022.121951.

Ayyoubi, S., Cerda, J.R., Fernández-García, R., Knief, P., Lalatsa, A., Healy, A.M., Serrano, D.R., 2021. 3D printed spherical mini-tablets: Geometry versus composition effects in controlling dissolution from personalised solid dosage forms. Int. J. Pharm. 597, 120336 https://doi.org/10.1016/J.IJPHARM.2021.120336.

Baird, J.A., Van Eerdenbrugh, B., Taylor, L.S., 2010. A classification system to assess the crystallization tendency of organic molecules from undercooled melts. J. Pharm. Sci. 99, 3787–3806. https://doi.org/10.1002/JPS.22197.

Balard, H., Brendle, E., Papier, E., 2000. Determination of the Acid/Base Properties of Solid Surface Using Inverse Gas Chromatography. In Advantages and Limitations. Acid-base interactions: relevance to adhesion science. VSP Int. Sci. Publ. 2, 299–316.

Bandari, S., Nyavanandi, D., Dumpa, N., Repka, M.A., 2021. Coupling hot melt extrusion and fused deposition modeling: Critical properties for successful performance. Adv. Drug Deliv. Rev. 172, 52–63. https://doi.org/10.1016/J.ADDR.2021.02.006.

Bhujbal, S.V., Mitra, B., Jain, U., Gong, Y., Agrawal, A., Karki, S., Taylor, L.S., Kumar, S., (Tony) Zhou, Q., 2021. Pharmaceutical amorphous solid dispersion: A review of manufacturing strategies. Acta Pharm. Sin. B 11, 2505–2536. https://doi.org/10.1016/J.APSB.2021.05.014.

Blaesi, H.A., Saka, N., 2024. Gastroretentive fibrous dosage forms for prolonged delivery of sparingly soluble tyrosine kinase inhibitors. Part 1: Dosage form design, and models of in vitro expansion, post-expansion mechanical strength, and drug release. Int. J. Pharm. 653, 123428 https://doi.org/10.1016/J.IJPHARM.2023.123428.

Brown, C., Chokshi, H., Nickerson, B., Reed, R., Rohrs, B., Shah, P., 2004. Dissolution testing ofpoorly soluble compounds. Pharm. Technol. 28, 56.

Cailleaux, S., Sanchez-Ballester, N.M., Gueche, Y.A., Bataille, B., Soulairol, I., 2021. Fused Deposition Modeling (FDM), the new asset for the production of tailored medicines. J. Control. Release 330, 821–841. https://doi.org/10.1016/J.JCONREL.2020.10.056.

Censi, R., Gigliobianco, M.R., Casadidio, C., Di Martino, P., 2018. Hot Melt Extrusion: Highlighting Physicochemical Factors to Be Investigated While Designing and Optimizing a Hot Melt Extrusion Process. Pharm. 2018, Vol. 10, Page 89 10, 89. 10.3390/PHARMACEUTICS10030089.

Chaturvedi, S., Lipszyc, D.H., Licht, C., Craig, J.C., Parekh, R., 2014. Pharmacological interventions for hypertension in children. Evidence-Based Child Heal. A Cochrane Rev. J. 9, 498–580. https://doi.org/10.1002/EBCH.1974.

DeBoyace, K., Wildfong, P.L.D., 2018. The Application of Modeling and Prediction to the Formation and Stability of Amorphous Solid Dispersions. J. Pharm. Sci. 107, 57–74. https://doi.org/10.1016/J.XPHS.2017.03.029.

Deon, M., dos Santos, J., de Andrade, D.F., Beck, R.C.R., 2022. A critical review of traditional and advanced characterisation tools to drive formulators towards the rational development of 3D printed oral dosage forms. Int. J. Pharm. 628, 122293 https://doi.org/10.1016/J.IJPHARM.2022.122293.

Ditzinger, F., Scherer, U., Schönenberger, M., Holm, R., Kuentz, M., 2019. Modified Polymer Matrix in Pharmaceutical Hot Melt Extrusion by Molecular Interactions with a Carboxylic Coformer. Mol. Pharm. 16, 141–150. https://doi.org/10.1021/ACS.MOLPHARMACEUT.8B00920/ASSET/IMAGES/MEDIUM/MP-2018-00920B_0011.GIF.

dos Santos, J., Balbinot, G. de S., Buchner, S., Collares, F.M., Windbergs, M., Deon, M., Beck, R.C.R., 2023. 3D printed matrix solid forms: Can the drug solubility and dose customisation affect their controlled release behaviour? Int. J. Pharm. X 5, 100153. https://doi.org/10.1016/J.IJPX.2022.100153.

Dumpa, N., Butreddy, A., Wang, H., Komanduri, N., Bandari, S., Repka, M.A., 2021. 3D printing in personalized drug delivery: An overview of hot-melt extrusion-based fused deposition modeling. Int. J. Pharm. 600, 120501 https://doi.org/10.1016/J.IJPHARM.2021.120501.

Dumpa, N.R., Bandari, S., Repka, M.A., 2020. Novel Gastroretentive Floating Pulsatile Drug Delivery System Produced via Hot-Melt Extrusion and Fused Deposition Modeling 3D Printing.

Essmann, U., Perera, L., Berkowitz, M.L., Darden, T., Lee, H., Pedersen, L.G., 1995. A smooth particle mesh Ewald method. J. Chem. Phys. 103, 8577–8593. https://doi.org/10.1063/1.470117.

Ferrero, C., Massuelle, D., Jeannerat, D., Doelker, E., 2013. Towards elucidation of the drug release mechanism from compressed hydrophilic matrices made of cellulose ethers. III. Critical use of thermodynamic parameters of activation for modeling the water penetration and drug release processes. J. Control. Release 170, 175–182. https://doi.org/10.1016/J.JCONREL.2013.05.016.

Gala, U.H., Miller, D.A., Williams, R.O., 2020. Harnessing the therapeutic potential of anticancer drugs through amorphous solid dispersions. Biochim. Biophys. Acta - Rev. Cancer 1873, 188319. https://doi.org/10.1016/J.BBCAN.2019.188319.

Ghamami, N., Chiang, S.H.Y., Dormuth, C., Wright, J.M., 2014. Time course for blood pressure lowering of dihydropyridine calcium channel blockers. Cochrane Database Syst. Rev. 2014 https://doi.org/10.1002/14651858.CD010052.PUB2/MEDIA/CDSR/CD010052/IMAGE_N/NCD010052-CMP-001-02.PNG.

Gokhale, A., 2014. Achieving zero-order release kinetics using multi-step diffusion-based drug delivery. Pharm. Technol. 38 (5).

Govender, R., Abrahmsén-Alami, S., Folestad, S., Larsson, A., 2020. High Content Solid Dispersions for Dose Window Extension: A Basis for Design Flexibility in Fused Deposition Modelling. Pharm. Res. 37 https://doi.org/10.1007/s11095-019-2720-6.

Govender, R., Abrahmsén-Alami, S., Folestad, S., Olsson, M., Larsson, A., 2021. Enabling modular dosage form concepts for individualized multidrug therapy: Expanding the design window for poorly water-soluble drugs. Int. J. Pharm. 602, 120625 https://doi.org/10.1016/J.IJPHARM.2021.120625.

Greenhalgh, D.J., Williams, A.C., Timmins, P., York, P., 1999. Solubility parameters as predictors of miscibility in solid dispersions. J. Pharm. Sci. 88, 1182–1190. https://doi.org/10.1021/js9900856.

Guo, W., Li, C., Du, P., Wang, Y., Zhao, S., Wang, J., Yang, C., 2020. Thermal properties of drug polymorphs: A case study with felodipine form I and form IV. J. Saudi Chem. Soc. 24, 474–483. https://doi.org/10.1016/j.jscs.2020.04.003.

Gupta, S.S., Solanki, N., Serajuddin, A.T.M., 2016. Investigation of Thermal and Viscoelastic Properties of Polymers Relevant to Hot Melt Extrusion, IV: Affinisol™ HPMC HME Polymers. AAPS PharmSciTech 17, 148–157. https://doi.org/10.1208/s12249-015-0426-6.

Han, R., Xiong, H., Ye, Z., Yang, Y., Huang, T., Jing, Q., Lu, J., Pan, H., Ren, F., Ouyang, D., 2019. Predicting physical stability of solid dispersions by machine learning techniques. J. Control. Release 311–312, 16–25. https://doi.org/10.1016/J.JCONREL.2019.08.030.

Higuchi, T., 1963. Mechanism of sustained-action medication. Theoretical analysis of rate of release of solid drugs dispersed in solid matrices. J. Pharm. Sci. 52, 1145–1149. https://doi.org/10.1002/jps.2600521210.

Huanbutta, K., Sangnim, T., 2019. Design and development of zero-order drug release gastroretentive floating tablets fabricated by 3D printing technology. J. Drug Deliv. Sci. Technol. 52, 831–837. https://doi.org/10.1016/j.jddst.2019.06.004.

Ilyés, K., Balogh, A., Casian, T., Igricz, T., Borbás, E., Démuth, B., Vass, P., Menyhárt, L., Kovács, N.K., Marosi, G., Tomuță, I., Nagy, Z.K., 2019. 3D floating tablets: Appropriate 3D design from the perspective of different in vitro dissolution testing methodologies. Int. J. Pharm. 567, 118433 https://doi.org/10.1016/j.ijpharm.2019.06.024.

Jakalian, A., Jack, D.B., Bayly, C.I., 2002. Fast, efficient generation of high-quality atomic charges. AM1-BCC model: II. Parameterization and Validation. J. Comput. Chem. 23, 1623–1641. https://doi.org/10.1002/JCC.10128.

Jankovic, S., Tsakiridou, G., Ditzinger, F., Koehl, N.J., Price, D.J., Ilie, A.R., Kalantzi, L., Kimpe, K., Holm, R., Nair, A., Griffin, B., Saal, C., Kuentz, M., 2019. Application of the solubility parameter concept to assist with oral delivery of poorly water-soluble drugs – a PEARRL review. J. Pharm. Pharmacol. 71, 441–463. https://doi.org/10.1111/JPHP.12948.

Jennotte, O., Koch, N., Lechanteur, A., Evrard, B., 2022. Development of amorphous solid dispersions of cannabidiol: Influence of the carrier, the hot-melt extrusion parameters and the use of a crystallization inhibitor. J. Drug Deliv. Sci. Technol. 71, 103372 https://doi.org/10.1016/j.jddst.2022.103372.

Karavas, E., Georgarakis, E., Bikiaris, D., 2006. Application of PVP/HPMC miscible blends with enhanced mucoadhesive properties for adjusting drug release in predictable pulsatile chronotherapeutics. Eur. J. Pharm. Biopharm. 64, 115–126. https://doi.org/10.1016/J.EJPB.2005.12.013.

Khizer, Z., Akram, M.R., Tahir, M.A., Liu, W., Lou, S., Conway, B.R., Ghori, M.U., 2023. Personalised 3D-Printed Mucoadhesive Gastroretentive Hydrophilic Matrices for Managing Overactive Bladder (OAB). Pharm. 2023, Vol. 16, Page 372 16, 372. 10.3390/PH16030372.

Kim, S.J., Lee, J.C., Ko, J.Y., Lee, S.H., Kim, N.A., Jeong, S.H., 2021. 3D-printed tablets using a single-step hot-melt pneumatic process for poorly soluble drugs. Int. J. Pharm. 595, 120257 https://doi.org/10.1016/J.IJPHARM.2021.120257.

Kimura, S., Ishikawa, T., Iwao, Y., Itai, S., Kondo, H., 2019. Fabrication of Zero-Order Sustained-Release Floating Tablets via Fused Depositing Modeling 3D Printer. Chem. Pharm. Bull. 67, 992–999. https://doi.org/10.1248/cpb.c19-00290.

Kirschner, K.N., Yongye, A.B., Tschampel, S.M., González-Outeiriño, J., Daniels, C.R., Foley, B.L., Woods, R.J., 2008. GLYCAM06: a generalizable biomolecular force field. Carbohydrates. J. Comput. Chem. 29, 622–655. https://doi.org/10.1002/JCC.20820.

Korsmeyer, R.W., Gurny, R., Doelker, E., Buri, P., Peppas, N.A., 1983. Mechanisms of solute release from porous hydrophilic polymers. Int. J. Pharm. 15, 25–35. https://doi.org/10.1016/0378-5173(83)90064-9.

Krieger, E., Vriend, G., 2014. YASARA View—molecular graphics for all devices—from smartphones to workstations. Bioinformatics 30, 2981–2982. https://doi.org/10.1093/BIOINFORMATICS/BTU426.

Lehmkemper, K., Kyeremateng, S.O., Heinzerling, O., Degenhardt, M., Sadowski, G., 2017. Impact of Polymer Type and Relative Humidity on the Long-Term Physical Stability of Amorphous Solid Dispersions. Mol. Pharm. 14, 4374–4386. https://doi.org/10.1021/ACS.MOLPHARMACEUT.7B00492/SUPPL_FILE/MP7B00492_SI_001.PDF.

Lu, Y., Chen, J., Yi, S., Xiong, S., 2019. Enhanced felodipine dissolution from high drug loading amorphous solid dispersions with PVP/VA and sodium dodecyl sulfate. J. Drug Deliv. Sci. Technol. 53, 101151 https://doi.org/10.1016/J.JDDST.2019.101151.

Lu, J., Cuellar, K., Hammer, N.I., Jo, S., Gryczke, A., Kolter, K., Langley, N., Repka, M.A., 2016. Solid-state characterization of Felodipine-Soluplus amorphous solid dispersions. Drug Dev. Ind. Pharm. 42, 485–496. https://doi.org/10.3109/03639045.2015.1104347.

Mahmah, O., Tabbakh, R., Kelly, A., Paradkar, A., 2014. A comparative study of the effect of spray drying and hot-melt extrusion on the properties of amorphous solid dispersions containing felodipine. J. Pharm. Pharmacol. 66, 275–284. https://doi.org/10.1111/JPHP.12099.

Mandal, U.K., Chatterjee, B., Senjoti, F.G., 2016. Gastro-retentive drug delivery systems and their in vivo success: A recent update. Asian J. Pharm. Sci. 10.1016/j.ajps.2016.04.007.

Marsac, P.J., Shamblin, S.L., Taylor, L.S., 2006. Theoretical and practical approaches for prediction of drug-polymer miscibility and solubility. Pharm. Res. 23, 2417–2426. https://doi.org/10.1007/S11095-006-9063-9/TABLES/2.

Marsac, P.J., Li, T., Taylor, L.S., 2009. Estimation of drug-polymer miscibility and solubility in amorphous solid dispersions using experimentally determined interaction parameters. Pharm. Res. 26, 139–151. https://doi.org/10.1007/S11095-008-9721-1/TABLES/4.

Mašková, E., Kubová, K., Raimi-Abraham, B.T., Vllasaliu, D., Vohlídalová, E., Turánek, J., Mašek, J., 2020. Hypromellose – A traditional pharmaceutical excipient with modern applications in oral and oromucosal drug delivery. J. Control. Release 324, 695–727. https://doi.org/10.1016/J.JCONREL.2020.05.045.

McDonagh, T., Belton, P., Qi, S., 2023. Manipulating drug release from 3D printed dual-drug loaded polypills using challenging polymer compositions. Int. J. Pharm. 637, 122895 https://doi.org/10.1016/J.IJPHARM.2023.122895.

Melocchi, A., Briatico-Vangosa, F., Uboldi, M., Parietti, F., Turchi, M., von Zeppelin, D., Maroni, A., Zema, L., Gazzaniga, A., Zidan, A., 2021. Quality considerations on the pharmaceutical applications of fused deposition modeling 3D printing. Int. J. Pharm. 592, 119901 https://doi.org/10.1016/J.IJPHARM.2020.119901.

Mohammadi-Jam, S., Waters, K.E., 2014. Inverse gas chromatography applications: A review. Adv. Colloid Interface Sci. 212, 21–44. https://doi.org/10.1016/J.CIS.2014.07.002.

Mora-Castaño, G., Millán-Jiménez, M., Caraballo, I., 2023. Hydrophilic High Drug-Loaded 3D Printed Gastroretentive System with Robust Release Kinetics. Pharm. 2023, Vol. 15, Page 842 15, 842. 10.3390/PHARMACEUTICS15030842.

Mora-Castaño, G., Millán-Jiménez, M., Linares, V., Caraballo, I., 2022. Assessment of the Extrusion Process and Printability of Suspension-Type Drug-Loaded AffinisolTM Filaments for 3D Printing. Pharmaceutics 14, 871. https://doi.org/10.3390/pharmaceutics14040871.

Newman, A. (Ed.), 2015. Pharmaceutical Amorphous Solid Dispersions. John Wiley & Sons Inc, Hoboken, New Yersey, p. 463.

Nimje, H.M., Oswal, R.J., Kshirsagar, S.S., Chavan, M., 2011. Spectrophotometric analysis for estimation of felodipine in tablet dosage form by calibration curve method. Res. J. Pharm. Technol. 4, 1805–1806.

Notario-Pérez, F., Cazorla-Luna, R., Martín-Illana, A., Ruiz-Caro, R., Tamayo, A., Rubio, J., Veiga, M.D., 2018. Optimization of tenofovir release from mucoadhesive vaginal tablets by polymer combination to prevent sexual transmission of HIV. Carbohydr. Polym. 179, 305–316. https://doi.org/10.1016/J.CARBPOL.2017.10.001.

Ouyang, D., 2012. Investigating the molecular structures of solid dispersions by the simulated annealing method. Chem. Phys. Lett. 554, 177–184. https://doi.org/10.1016/J.CPLETT.2012.10.056.

Structured Development Approach for Amorphous Systems volume 3, 2016, 329–382.

Palazi, E., Karavas, E., Barmpalexis, P., Kostoglou, M., Nanaki, S., Christodoulou, E., Bikiaris, D.N., 2018. Melt extrusion process for adjusting drug release of poorly water soluble drug felodipine using different polymer matrices. Eur. J. Pharm. Sci. 114, 332–345. https://doi.org/10.1016/J.EJPS.2018.01.004.

Parulski, C., Gresse, E., Jennotte, O., Felten, A., Ziemons, E., Lechanteur, A., Evrard, B., 2022. Fused deposition modeling 3D printing of solid oral dosage forms containing amorphous solid dispersions: How to elucidate drug dissolution mechanisms through surface spectral analysis techniques? Int. J. Pharm. 626, 122157 https://doi.org/10.1016/J.IJPHARM.2022.122157.

Patil, H., Tiwari, R.V., Repka, M.A., 2016. Hot-Melt Extrusion: from Theory to Application in Pharmaceutical Formulation. AAPS PharmSciTech 17, 20–42. https://doi.org/10.1208/s12249-015-0360-7.

Pereira, G.G., Figueiredo, S., Fernandes, A.I., Pinto, J.F., 2020. Polymer Selection for Hot-Melt Extrusion Coupled to Fused Deposition Modelling in Pharmaceutics. Pharm. 2020, Vol. 12, Page 795 12, 795. 10.3390/PHARMACEUTICS12090795.

Pietrzak, K., Isreb, A., Alhnan, M.A., 2015. A flexible-dose dispenser for immediate and extended release 3D printed tablets. Eur. J. Pharm. Biopharm. 96, 380–387. https://doi.org/10.1016/J.EJPB.2015.07.027.

Prasad, E., Islam, M.T., Goodwin, D.J., Megarry, A.J., Halbert, G.W., Florence, A.J., Robertson, J., 2019. Development of a hot-melt extrusion (HME) process to produce drug loaded AffinisolTM 15LV filaments for fused filament fabrication (FFF) 3D printing. Addit. Manuf. 29, 100776 https://doi.org/10.1016/j.addma.2019.06.027.

Reynolds, T.D., Mitchell, S.A., Balwinski, K.M., 2002. Investigation of the Effect of Tablet Surface Area/Volume on Drug Release from Hydroxypropylmethylcellulose Controlled-Release Matrix Tablets. Drug Dev. Ind. Pharm. 28, 457–466. https://doi.org/10.1081/DDC-120003007.

Ritger, P.L., Peppas, N.A., 1987. A simple equation for description of solute release I. Fickian and non-fickian release from non-swellable devices in the form of slabs, spheres, cylinders or discs. J. Control. Release 5, 23–36. https://doi.org/10.1016/0168-3659(87)90034-4.

Rumondor, A.C.F., Taylor, L.S., 2010. Effect of polymer hygroscopicity on the phase behavior of amorphous solid dispersions in the presence of moisture. Mol. Pharm. 7, 477–490. https://doi.org/10.1021/MP9002283/ASSET/IMAGES/MEDIUM/MP-2009-002283_0012.GIF.

Rumondor, A.C.F., Stanford, L.A., Taylor, L.S., 2009. Effects of polymer type and storage relative humidity on the kinetics of felodipine crystallization from amorphous solid dispersions. Pharm. Res. 26, 2599–2606. https://doi.org/10.1007/S11095-009-9974-3/FIGURES/8.

Saboo, S., Bapat, P., Moseson, D.E., Kestur, U.S., Taylor, L.S., 2021. Exploring the role of surfactants in enhancing drug release from amorphous solid dispersions at higher drug loadings. Pharmaceutics 13, 735. https://doi.org/10.3390/PHARMACEUTICS13050735/S1.

Sadia, M., Arafat, B., Ahmed, W., Forbes, R.T., Alhnan, M.A., 2018. Channelled tablets: An innovative approach to accelerating drug release from 3D printed tablets. J. Control. Release 269, 355–363. https://doi.org/10.1016/j.jconrel.2017.11.022.

Sandoval, H.P., Baema, Y., Aragón, M., Rosas, J., Ponce D'León, L., 2008. Mecanismos generales de cesión de principios activos a partir de matrices monolíticas hidrofílicas preparadas con éteres de celulosa. Rev. Colomb. Cienc. Quím. Farm. 37 (2), 105–121.

Select Committee on GRAS Substances (SCOGS), 1973. Report 25: Evaluation of the health aspects of cellulose and certain cellulose derivatives as food ingredients.

Shojaie, F., Ferrero, C., Caraballo, I., 2023. Development of 3D-Printed Bicompartmental Devices by Dual-Nozzle Fused Deposition Modeling (FDM) for Colon-Specific Drug Delivery. Pharmaceutics 15, 2362. https://doi.org/10.3390/PHARMACEUTICS15092362/S1.

Skowyra, J., Pietrzak, K., Alhnan, M.A., 2015. Fabrication of extended-release patient-tailored prednisolone tablets via fused deposition modelling (FDM) 3D printing. Eur. J. Pharm. Sci. 68, 11–17. https://doi.org/10.1016/J.EJPS.2014.11.009.

Solanki, N.G., Tahsin, M., Shah, A.V., Serajuddin, A.T.M., 2018. Formulation of 3D Printed Tablet for Rapid Drug Release by Fused Deposition Modeling: Screening Polymers for Drug Release, Drug-Polymer Miscibility and Printability. J. Pharm. Sci. 107, 390–401. https://doi.org/10.1016/j.xphs.2017.10.021.

Tambe, S., Jain, D., Meruva, S.K., Rongala, G., Juluri, A., Nihalani, G., Mamidi, H.K., Nukala, P.K., Bolla, P.K., 2022. Recent Advances in Amorphous Solid Dispersions: Preformulation, Formulation Strategies, Technological Advancements and Characterization. Pharm. 2022, Vol. 14, Page 2203 14, 2203. 10.3390/PHARMACEUTICS14102203.

Tambe, S., Jain, D., Agarwal, Y., Amin, P., 2021. Hot-melt extrusion: Highlighting recent advances in pharmaceutical applications. J. Drug Deliv. Sci. Technol. 63, 102452 https://doi.org/10.1016/j.jddst.2021.102452.

Tan, D.K., Maniruzzaman, M., Nokhodchi, A., 2018. Advanced Pharmaceutical Applications of Hot-Melt Extrusion Coupled with Fused Deposition Modelling (FDM) 3D Printing for Personalised Drug Delivery. Pharm. 2018, Vol. 10, Page 203 10, 203. 10.3390/PHARMACEUTICS10040203.

Thakkar, R., Thakkar, R., Pillai, A., Ashour, E.A., Repka, M.A., 2020. Systematic screening of pharmaceutical polymers for hot melt extrusion processing: a comprehensive review. Int. J. Pharm. 576, 118989 https://doi.org/10.1016/J.IJPHARM.2019.118989.

Van Krevelen, D.W., Te Nijenhuis, K., 2009. Cohesive Properties and Solubility. Prop. Polym. 189–227 https://doi.org/10.1016/B978-0-08-054819-7.00007-8.

Verstraete, G., Samaro, A., Grymonpré, W., Vanhoorne, V., Van Snick, B., Boone, M.N., Hellemans, T., Van Hoorebeke, L., Remon, J.P., Vervaet, C., 2018. 3D printing of high drug loaded dosage forms using thermoplastic polyurethanes. Int. J. Pharm. 536, 318–325. https://doi.org/10.1016/j.ijpharm.2017.12.002.

Vo, A.Q., Feng, X., Pimparade, M., Ye, X., Kim, D.W., Martin, S.T., Repka, M.A., 2017. Dual-mechanism gastroretentive drug delivery system loaded with an amorphous solid dispersion prepared by hot-melt extrusion. Eur. J. Pharm. Sci. 102, 71–84. https://doi.org/10.1016/j.ejps.2017.02.040.

Voelkel, A., Strzemiecka, B., Adamska, K., Milczewska, K., 2009. Inverse gas chromatography as a source of physiochemical data. J. Chromatogr. A 1216, 1551–1566. https://doi.org/10.1016/J.CHROMA.2008.10.096.

Wang, J., Wolf, R.M., Caldwell, J.W., Kollman, P.A., Case, D.A., 2004. Development and testing of a general amber force field. J. Comput. Chem. 25, 1157–1174. https://doi.org/10.1002/JCC.20035.

Xiang, T.X., Anderson, B.D., 2017. Molecular Dynamics Simulation of Amorphous Hydroxypropylmethylcellulose and Its Mixtures With Felodipine and Water. J. Pharm. Sci. 106, 803–816. https://doi.org/10.1016/j.xphs.2016.10.026.

Yani, Y., Kanaujia, P., Chow, P.S., Tan, R.B.H., 2017. Effect of API-Polymer Miscibility and Interaction on the Stabilization of Amorphous Solid Dispersion: A Molecular Simulation Study. Ind. Eng. Chem. Res. 56, 12698–12707. https://doi.org/10.1021/acs.iecr.7b03187.

Yi, S., Wang, J., Lu, Y., Ma, R., Gao, Q., Liu, S., Xiong, S., 2019. Novel Hot Melt Extruded Matrices of Hydroxypropyl Cellulose and Amorphous Felodipine-Plasticized Hydroxypropyl Methylcellulose as Controlled Release Systems. AAPS PharmSciTech 20, 1–14. https://doi.org/10.1208/S12249-019-1435-7.

Zhang, J., Yang, W., Vo, A.Q., Feng, X., Ye, X., Kim, D.W., Repka, M.A., 2017. Hydroxypropyl methylcellulose-based controlled release dosage by melt extrusion and 3D printing: Structure and drug release correlation. Carbohydr. Polym. 177, 49–57. https://doi.org/10.1016/j.carbpol.2017.08.058.

Zhang, J., Guo, M., Luo, M., Cai, T., 2023. Advances in the development of amorphous solid dispersions: The role of polymeric carriers. Asian J. Pharm. Sci. 18, 100834 https://doi.org/10.1016/J.AJPS.2023.100834.

Zhao, Y.N., Xu, X., Wen, N., Song, R., Meng, Q., Guan, Y., Cheng, S., Cao, D., Dong, Y., Qie, J., Liu, K., Zhang, Y., 2017. A Drug Carrier for Sustained Zero-Order Release of Peptide Therapeutics. Sci. Reports 2017 71 7, 1–9. 10.1038/s41598-017-05898-6.

Zhao, X., Wei, W., Niu, R., Li, Q., Hu, C., Jiang, S., 2022. 3D Printed Intragastric Floating and Sustained-Release Tablets with Air Chambers. J. Pharm. Sci. 111, 116–123. https://doi.org/10.1016/J.XPHS.2021.07.010.